JOURNAL OF GEOPHYSICAL RESEARCH, VOL. 103, NO. C1, PAGES 1343-1362, JANUARY 15, 1998

A new method to determine the mean sea surface dynamic topography from satellite altimeter observations

R. C. V. Feron,[1] W. P. M. De Ruijter, and P. J. van Leeuwen

Institute for Marine and Atmospheric Research, Utrecht University, Utrecht, Netherlands

Abstract. A method is presented to calculate mean sea surface dynamic topography from satellite altimeter observations of its temporal variability. Time averaging of a simplified version of the quasi-geostrophic potential vorticity equation for the upper ocean layer results in a differential equation for the averaged relative vorticity in which the mean divergence of the eddy vorticity fluxes acts as a source or sink. The essential part is that these eddy fluxes can be determined from the altimeter observations. Consequently, no parameterisations appear in the averaged vorticity equation. From the average vorticity field, surface geostrophic velocities and related mean dynamic sea surface topography can then simply be derived. The usefulness of the method is established using "perfect" data, namely numerical output from the United Kingdom Fine Resolution Antarctic Model. The method appears applicable to areas of the ocean with strong enough mesoscale variability such as the major western boundary currents and their extensions and to frontal regions of the Antarctic Circumpolar Current. Quite realistic results are presented for active regions of the world ocean. Results are compared with hydrographic observations for the major western boundary current extensions of the Southern Ocean. An important application is to combine the newly derived averaged flow field with the observed eddy field to derive the total time-varying geostrophic surface velocity field. As a striking example this is applied to the Agulhas Current retroflection, where the repeated shedding of large rings can now be synoptically reconstructed as a continuous process.

1. Introduction

The expected accuracy of recent marine geoid models at scales shorter than about 4000 km is still at the decimeter level. This is not adequate for determination of the mean global ocean circulation at these length scales [*Chelton*, 1988; *Nerem et al.*, 1990; *Fu et al.*, 1996]. The only direct way to use satellite altimeter observations for determining the mean global ocean circulation is to combine the altimeter observations with a geoid model with centimeter precision at all wavelengths.

A direct consequence of the inability to extract the MSSDT, η, is that the high measurement precision and accuracy (3-5 cm) of altimeters can only be optimally exploited to determine the time-variable sea surface topography η'. Assuming geostrophy, η' can only be used to compute the time-variable surface velocity field. The possibility of accurately observing ocean variability in the mesoscale range (10-100 days, 50-500 km) has led to progress in understanding and mapping the ocean eddy field [e.g., *Cheney et al.*, 1983; *Wakker et al.*, 1990; *Tai and White*, 1988; *Shum et al.*, 1990; *Gordon and Haxby*, 1990; *Feron et al.*, 1992]. However, the inability to determine the MSSDT, and thus the mean flow field, makes interpretation of altimeter observations very difficult. For instance, it is impossible to distinguish between ring formations and current meanders, and ring trajectories are hard to study in regions with strong mean currents. Methods to improve interpretation of altimeter time series are based on additional information, e.g., other independent observations. *Vazquez et al.* [1990] combined Geosat data with observations of sea surface temperature in the Gulf Stream area. Other studies [e.g., *Tai and White*, 1988; *Willebrand et al.*, 1990; *Gordon and Haxby*, 1990; *Ichikawa and Imawaki*, 1994] combined hydrographic data and/or surface drifter buoys with Geosat data to study rings detached from the mean flow. *Kelly and*

[1] Now at Survey Department, Rijkswaterstaat, Delft, Netherlands

Paper number 97JC00389.
0148-0227/98/97JC-00389$09.00

Gille [1990] and *Qiu et al.* [1991] investigated the mean flow in the Gulf Stream and Kuroshio Extension, respectively, by fitting a synthetic current's height profile to Geosat residual height data along individual tracks. Their results were found to be in remarkable agreement with hydrographic and acoustic Doppler current profiles [e.g., *Kelly et al.*, 1991; *Teage et al.*, 1990]. More recently, *Gille* [1994] used the same technique for mapping the Antarctic Circumpolar Current. Both the Subantarctic Front and the Polar Front could be determined and analyzed from Geosat altimeter data.

Another way to improve interpretation is application of statistical techniques that analyse decorrelation in time and space [e.g., *Feron et al.*, 1992].

Two methods are presently in use to estimate the long wavelength part of the MSSDT from altimeter observations. The first method simultaneously adjusts the gravity field and determines the MSSDT. This so-called integrated least squares approach is successful for wavelengths larger than roughly 4000 km [e.g., *Marsh et al.*, 1990; *Engelis and Knudsen*, 1989; *Nerem et al.*, 1990; *Visser*, 1992]. The second method has become increasingly more interesting due to the very accurately known orbit of the recent TOPEX/POSEIDON satellite mission. Due to that high precision (3-5 cm in radial position), height observations can simply be subtracted from the best available geoid model to give an estimate of MSSDT [e.g., *Minster et al.*, 1993; *Naeije et al.*, 1993; *Fu et al.*, 1996]. This approach is beginning to work because of improvements in the accuracy of the latest geoid models. A limiting factor in both approaches is that the errors in the gravity model are larger than the MSSDT signal for wavelengths smaller than approximately 4000 km. The short wavelength part of the MSSDT can therefore not be separated from the gravity field.

In the next section the observations are described. In this paper a method is proposed to estimate MSSDT from satellite altimeter observations of sea surface variability (section 3). It is based on time averaging of a simplified vorticity equation in which sea surface topography is separated in a mean and a time-varying part (section 2).

The approximation is valid only for ocean areas with strong mesoscale variability such as the major western boundary currents and the jets within the Antarctic Circumpolar Current. Application of this method shows surprisingly promising results (section 4) as compared to hydrographic observations in three major western boundary currents of the Southern Ocean. A more detailed comparison between climatology and the new MSSDT fields is achieved by comparing meridional sections (section 6). Section 7 shows how mean and time-variable flow can be combined to determine absolute time-varying sea surface topography fields from the altimetry time series. This is applied to determine ring shedding in the Agulhas Retroflection area. In the concluding section the method, its results, and limitations are summarized and discussed.

2. Data

The geostrophic surface flow and sea surface dynamic topography, η, can be decomposed in a time-averaged mostly large-scale part ($\overline{u}$ and $\overline{v}$) and a time-variable mesoscale part (u' and v'),

$$\begin{aligned} \eta &= \overline{\eta} + \eta' \\ u &= \overline{u} + u' \\ v &= \overline{v} + v' \end{aligned}$$

If the observed time series ($\eta'(x, y, t)$) are sufficiently long in time, realistic estimates of the time-variable velocity (cross) covariances, $\overline{u'u'}$, $\overline{v'v'}$, and $\overline{u'v'}$, can be computed (Plate 1). The overbar indicates time averaging, in this study over 3 years, e.g., the complete Geosat Exact Repeat Mission (ERM) data set. Geosat suffered from data loss in certain regions during the third year, something that should be kept in mind when looking at the results. These eddy stress terms can be derived from satellite altimeter anomalies under the assumption of geostrophy (Plate 1) and are computed at an equidistant $\Delta x = \Delta y = 0.5^o$ grid. They hold statistical information of the mesoscale turbulence over the total averaging period [e.g., *Holloway and Kristmannsson*, 1984; *Holopainen*, 1978; *Hoskins et al.*, 1983].

Gridding has been done with a 1^o decorrelation distance. Obviously, the 0.5^o grid oversampled the spatial scales Geosat is able to resolve. This oversampling is chosen for computational purposes. The spatial derivatives, necessary to compute the above mentioned eddy stress terms, are derived over a 1^o spatial distance both in longitudinal and latitudinal direction. Let ζ' be the time-variable relative vorticity:

$$\zeta' = \frac{\partial v'}{\partial x} - \frac{\partial u'}{\partial y} \tag{1}$$

The geostrophic time-variable flow is divergence free. This allows the relative vorticity eddy flux terms $\overline{u'\zeta'}$ and $\overline{v'\zeta'}$ to be expressed in terms of the eddy stresses:

$$\overline{u'\zeta'} = \frac{\partial[\frac{1}{2}(\overline{v'v'} - \overline{u'u'})]}{\partial y} + \frac{\partial\overline{u'v'}}{\partial x} \tag{2}$$

$$\overline{v'\zeta'} = \frac{\partial[\frac{1}{2}(\overline{v'v'} - \overline{u'u'})]}{\partial x} - \frac{\partial\overline{u'v'}}{\partial y} \tag{3}$$

Computing $\overline{u'\zeta'}$ and $\overline{v'\zeta'}$ from (2) and (3) is very efficient and less sensitive to measurement noise because the gradients are computed from the time-averaged eddy stress terms. The spatial distribution of these mean relative vorticity eddy flux terms (Plate 2, top two panels) shows clear inhomogeneities. In such regions

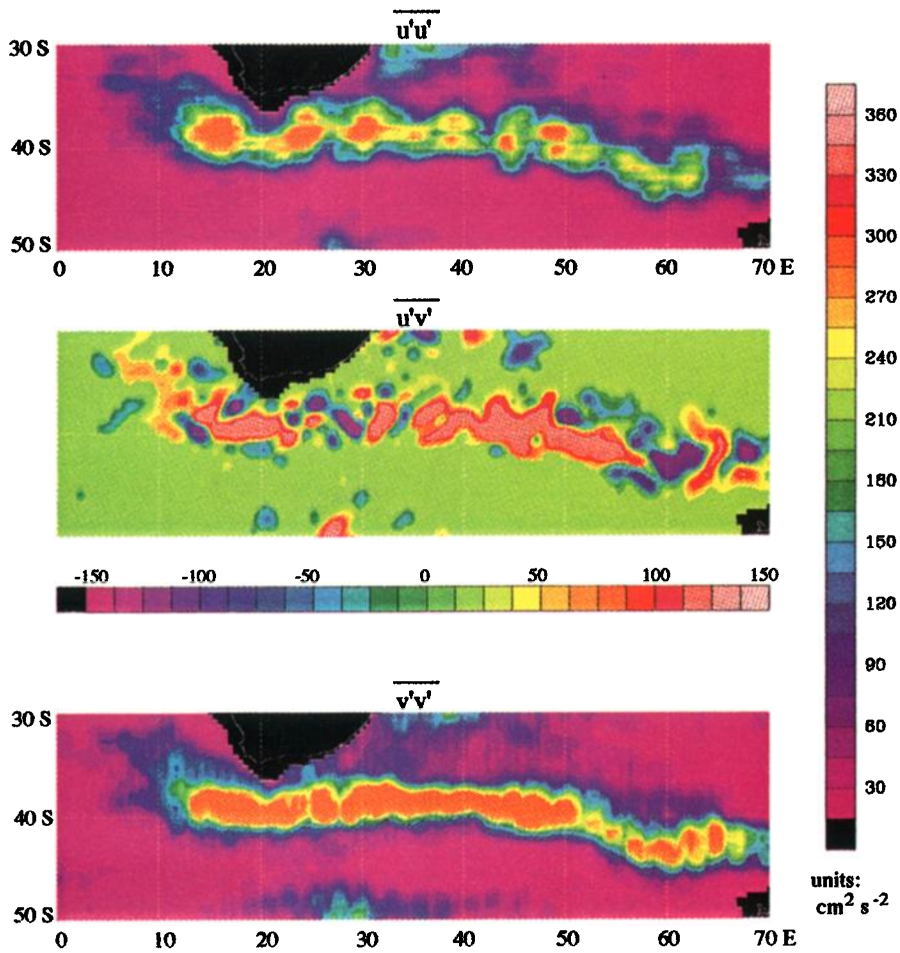

Plate 1. Horizontal eddy stress terms in the Southern Ocean computed from almost 3 years of Geosat altimeter data. Ocean regions with strong mesoscale activity correlate with large eddy stresses (units are $cm^2\ s^{-2}$).

the divergence of these average eddy fluxes is nonzero, so it can act to modify the mean flow (Plate 2, bottom panel).

3. The Method

3.1. The Vorticity Balance

Areas with larger eddy variability are the separation regions of the major western boundary currents and their extensions (Plate 1). There the divergence of the mean relative vorticity eddy flux has values of order $10^{-12}\ s^{-2}$ (Plate 2, bottom panel). This is an order of magnitude larger than vorticity input at the surface by the wind (O $(10^{-13} s^{-2})$ [e.g., *Hellermann and Rosenstein*, 1983]) and of the same order as the advection of planetary vorticity ($\beta\overline{v} = 1.6 \times 10^{-12}\ s^{-2}$ for $\overline{v} = 0.1$ m s^{-1} and $\beta = 1.6 \times 10^{-11}\ m^{-1}\ s^{-1}$ is the variation with latitude of the Coriolis parameter). A measure for the relative importance of advection of relative vorticity is the β Rossby number $\overline{v}/\beta L^2$. With the above characteristic value for β and $\overline{v}$ and a length scale $L = 10^5$ m, this Rossby number is of order 1. An estimate of the relative importance of stretching is obtained by considering the potential vorticity equation for the upper ocean layer

$$\frac{d}{dt}\left(\frac{\zeta + f}{h}\right) = 0 \tag{4}$$

where ζ is relative vorticity, f is the Coriolis parameter, and h is the upper layer thickness. If lower layer velocities are relatively small, than it can be shown that in the time-averaged form of the potential vorticity equation, an estimate of the stretching is given by

$$-\frac{\rho}{\overline{h}\Delta\rho}\overline{\zeta'\frac{\partial\eta'}{\partial t}} \sim -\overline{\zeta'\frac{\partial\eta'}{\partial t}} \tag{5}$$

for characteristic values: $\overline{h} = 10^3$ m, the density, $\rho = 10^3\ kg\ m^{-3}$, density difference between upper and lower layer, $\Delta\rho = 1\ kg\ m^{-3}$. Consequently, the effect of stretching can be estimated from the data. In the areas with large eddy variability this term appears to be of order $10^{-14}\ s^{-2}$ (Plate 3 and Table 1), so it is at least an

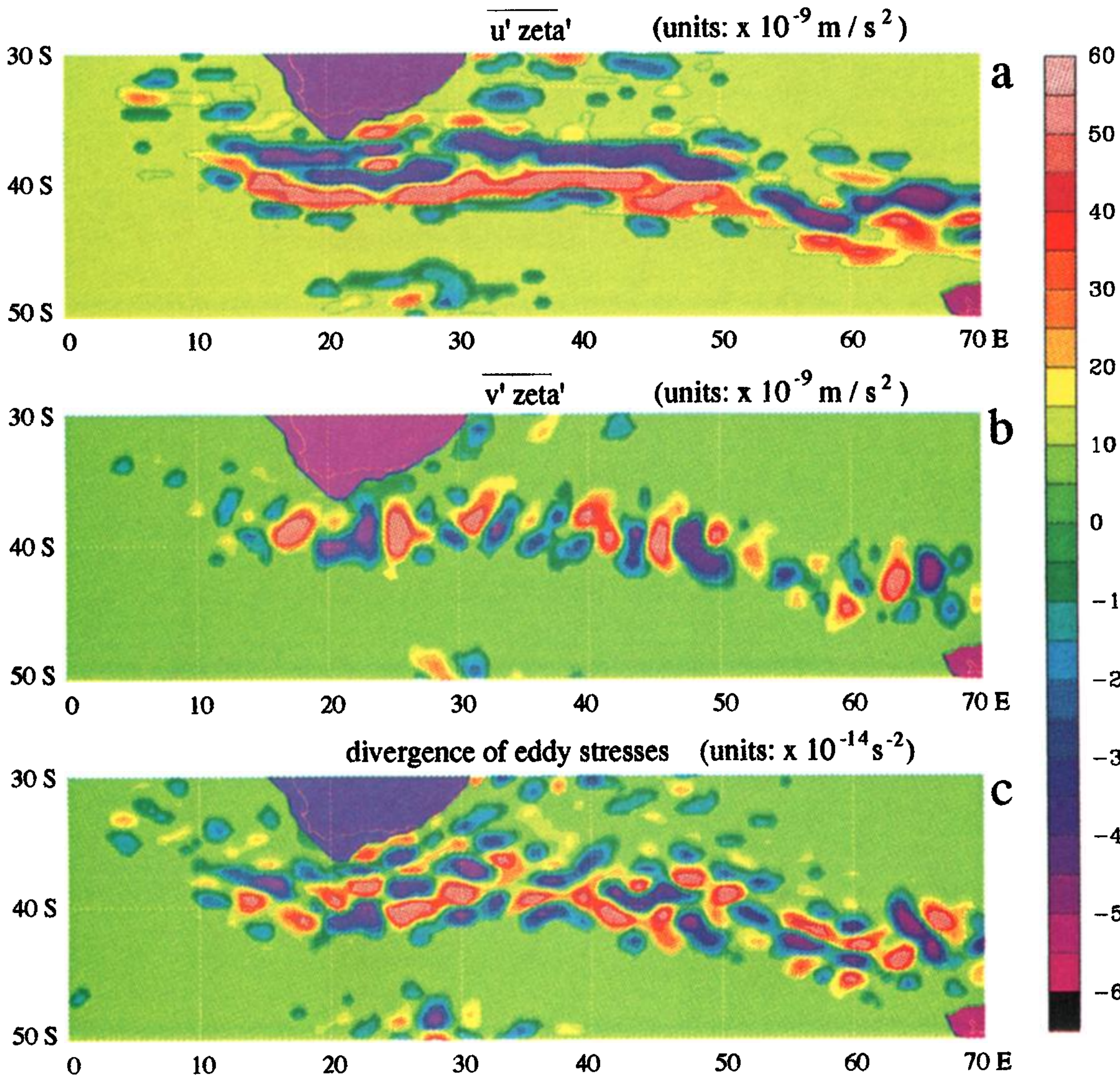

Plate 2. The vorticity eddy flux stress terms $\overline{u'\zeta'}$ and $\overline{v'\zeta'}$ ($\times 10^{-9}$m s^{-2}) in the Southern Ocean computed from almost 3 years of Geosat altimeter data. The bottom panel shows the divergence of these eddy flux stress terms, i.e., $(\partial(\overline{u'\zeta'})/\partial x + \partial(\overline{v'\zeta'})/\partial y)$ (units are $\times 10^{-14}$ s^{-2}).

order of magnitude smaller than the above-mentioned processes.

Obviously, the above assumptions are only approximately valid in the areas we consider. It should be considered as a first step in the development of a method, where the question to be addressed here is whether it leads to reasonable results. If that is already the case in this simple context, than it is worthwhile to develop and refine further the method and include a more complete model. So the starting point is the vorticity equation for the upper layer:

$$\frac{d(\overline{\zeta} + \zeta' + f)}{dt} = 0 \tag{6}$$

where

$$\frac{d}{dt} \equiv \frac{\partial}{\partial t} + u\frac{\partial}{\partial x} + v\frac{\partial}{\partial y} \tag{7}$$

$$u = -\frac{g}{f}\frac{\partial \eta}{\partial y}, \quad v = \frac{g}{f}\frac{\partial \eta}{\partial x} \tag{8}$$

Averaging (6) in time gives

$$\overline{u}\frac{\partial \overline{\zeta}}{\partial x} + \overline{v}\frac{\partial \overline{\zeta}}{\partial y} + \overline{v}\beta = -\frac{\partial}{\partial x}\overline{u'\zeta'} - \frac{\partial}{\partial y}\overline{v'\zeta'} \tag{9}$$

In this balance between mean relative vorticity advection by the mean flow, planetary vorticity advection, and the divergence of the average eddy fluxes of relative vorticity, the latter term is estimated by satellite altimetry (Plate 2, bottom panel). So, within this model context a solution can be determined without parameterizing the eddy fluxes.

Using geostrophy, this equation can be written as a third-order nonlinear differential equation in η (the MSSDT):

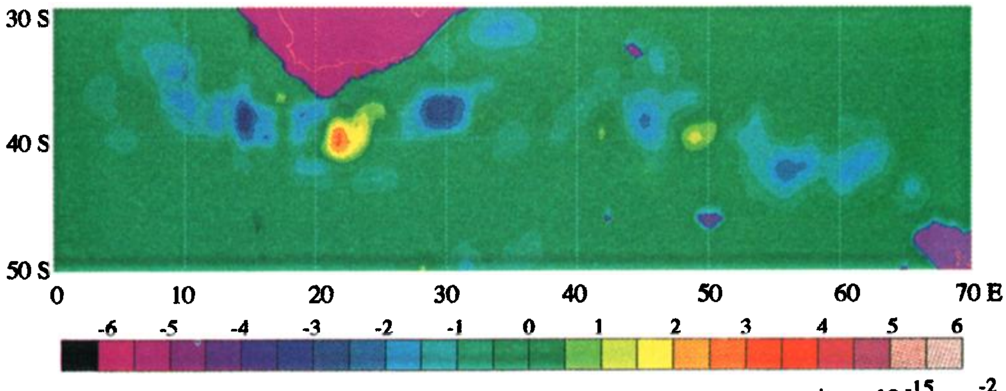

Plate 3. The $\overline{\zeta'\partial\eta'/\partial t}$ derived from almost 3 years of Geosat altimeter data (units are $\times 10^{-15}$ m s^{-2}).

$$-\frac{g}{f}\frac{\partial\overline{\eta}}{\partial y}\frac{\partial\Delta\overline{\eta}}{\partial x}+\frac{g}{f}\frac{\partial\overline{\eta}}{\partial x}\frac{\partial\Delta\overline{\eta}}{\partial y}+\beta\frac{\partial\overline{\eta}}{\partial x}= \overline{\frac{g}{f}\frac{\partial\eta'}{\partial y}\frac{\partial\Delta\eta'}{\partial x}}-\overline{\frac{g}{f}\frac{\partial\eta'}{\partial x}\frac{\partial\Delta\eta'}{\partial y}} \qquad (10)$$

Instead of directly solving this nonlinear equation, we follow an iterative two-step approach which first solves $\overline{\zeta}$ and than $\overline{\eta}$.

3.2. The Approximate Solution for the Mean Dynamic Topography

Equation (9) can be used to form the following set of equations:

$$\overline{u}_*\underline{\frac{\partial\overline{\zeta}}{\partial x}}+\overline{v}_*\underline{\frac{\partial\overline{\zeta}}{\partial y}}\simeq-\overline{v}_*\beta-\frac{\partial}{\partial x}\overline{u'\zeta'}-\frac{\partial}{\partial y}\overline{v'\zeta'} \qquad (11)$$

$$\underline{\frac{\partial\overline{\zeta}}{\partial x}}\simeq\frac{\partial\overline{\zeta}_*}{\partial x} \qquad (12)$$

$$\underline{\frac{\partial\overline{\zeta}}{\partial y}}\simeq\frac{\partial\overline{\zeta}_*}{\partial y} \qquad (13)$$

where the two underlined terms will be regarded as unknowns that can be approximated via a least squares procedure. Here $\overline{u}_*$, $\overline{v}_*$, $\partial\overline{\zeta_*}/\partial x$, and $\partial\overline{\zeta_*}/\partial y$ are initially estimated from the *Levitus* [1982] climatology. By adding (12) and (13) to (9), the system becomes overdetermined and the least squares approximation for $\partial\overline{\zeta}/\partial x$ and $\partial\overline{\zeta}/\partial y$ can be determined.

Because the vorticity equation has been derived using important simplifications and the climatology is known to be uncertain, we give equal weights to all three equations. Solving the above set of equations results in new estimates for the unknowns consisting of an optimal combination of the vorticity balance (which include the altimeter observations of horizontal eddy vorticity fluxes) and climatology.

Once new values for $\partial\overline{\zeta}/\partial x$ and $\partial\overline{\zeta}/\partial y$ have been determined, they are differentiated with respect to x and y, respectively, and summed to find Q:

$$Q=\frac{\partial^2\overline{\zeta}}{\partial x\partial x}+\frac{\partial^2\overline{\zeta}}{\partial y\partial y} \qquad (14)$$

from which $\overline{\zeta}$ can be solved straightforwardly using, e.g., iterative multigrid methods [e.g., *Wesseling*, 1992].

Table 1. Estimated Maximum and Minimum for Different Terms in the Potential Vorticity Equation

Variable	Low/Noise	High/Maximum	Units
$u' \sim v' \sim \overline{u} \sim \overline{v}$	0.05	0.5	m s^{-1}
$\partial\overline{u}/\partial x \sim \partial\overline{u}/\partial y \sim \partial\overline{v}/\partial x \sim \partial\overline{v}/\partial y$	1×10^{-7}	2×10^{-6}	s^{-1}
$\zeta' \sim \overline{\zeta}$	1×10^{-7}	2×10^{-6}	s^{-1}
$\partial\overline{\zeta}/\partial x \sim \partial\overline{\zeta}/\partial y \sim \partial\zeta'/\partial x \sim \partial\zeta'/\partial y$	1×10^{-12}	2×10^{-11}	s^{-1} m^{-1}
β		1.6×10^{-11}	m^{-1} s^{-1}
$\overline{u'\zeta'} \sim \overline{v'\zeta'}$	1×10^{-8}	1×10^{-7}	m s^{-2}
$\overline{\zeta'\partial\eta'/\partial t}$	1×10^{-16}	1×10^{-14}	m s^{-2}
$\partial(\overline{u'\zeta'})/\partial x \sim \partial(\overline{v'\zeta'})/\partial y$	1×10^{-14}	1×10^{-12}	s^{-2}

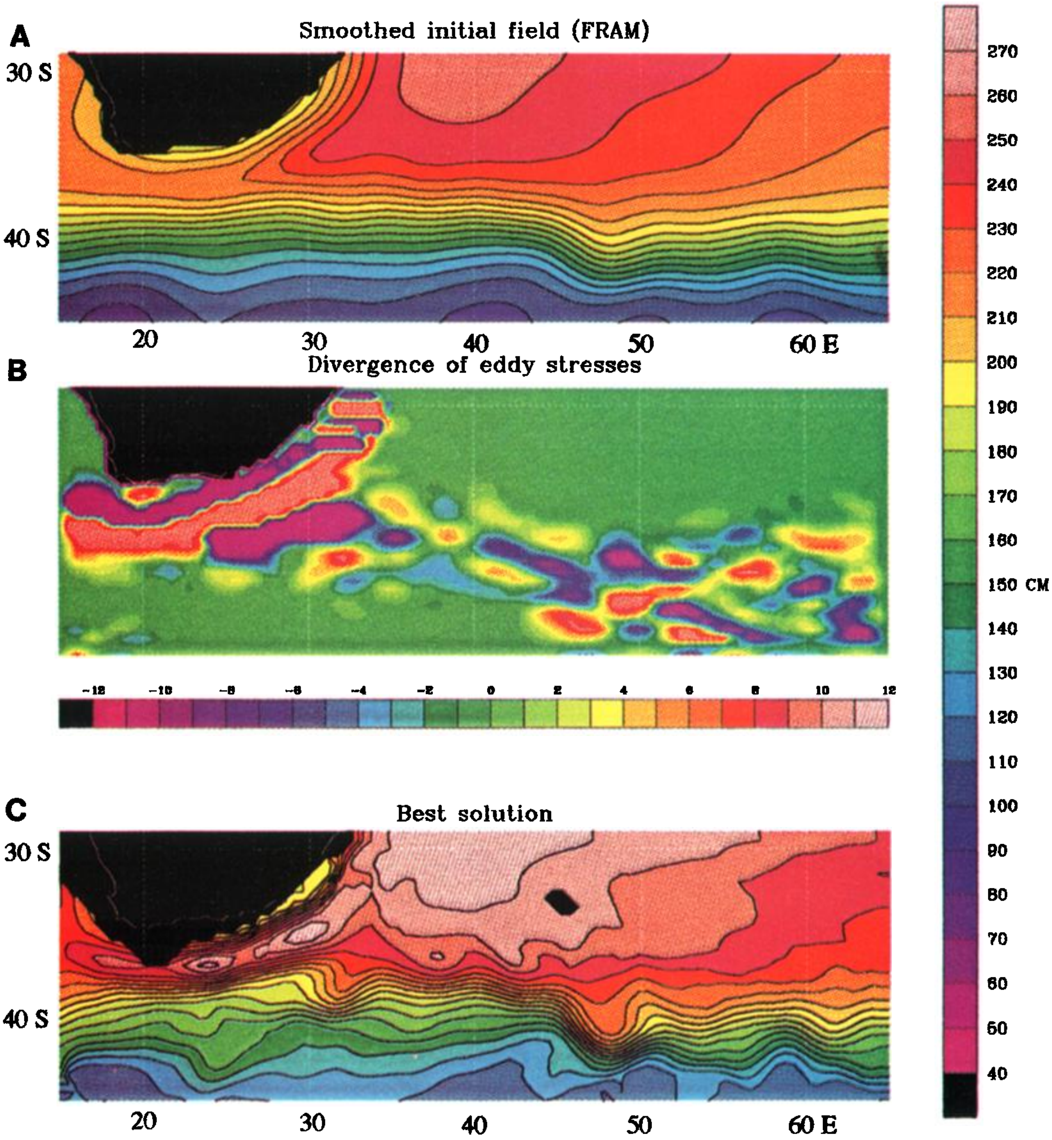

Plate 4. (a) Smoothed initial field (FRAM) derived from a 2-year averaged FRAM dynamic topography. (b) The divergence of FRAM eddy flux stresses (units are $\times 10^{-13}$ s^{-2}). (c) New MSSDT solution from the potential vorticity approach (units, see right-hand side fo vertical color bar).

The horizontal resolution is chosen according to the observations, e.g., $\Delta x = \Delta y = 0.5°$. Necessary boundary conditions for this elliptic differential equation are taken from climatology and prescribed on closed contours where the sea surface variability equals 7 cm. Results of changing this boundary condition showed more sensitivity to the smoothness of the contour than to the magnitude of variability. Those contours enclose ocean regions where the ocean signal is large compared to the altimeter noise level which means that the right-hand side of (9) can be determined with confidence.

$$\overline{\zeta}_{\text{bound}} = \overline{\zeta}_{\text{Lev}} \qquad |_{\text{variability}=7\text{ cm}} \tag{15}$$

The second step in the procedure is to derive $\overline{\eta}$ from the improved time-averaged relative vorticity $\overline{\zeta}$. Using the definition of the relative vorticity of the stationary geostrophic flow field in terms of the mean sea surface dynamic topography, we can write

$$\overline{\zeta} = \frac{g}{f}\frac{\partial^2 \overline{\eta}}{\partial x \partial x} + \frac{g}{f}\frac{\partial^2 \overline{\eta}}{\partial y \partial y} \tag{16}$$

from which $\overline{\eta}$ can be easily solved. The boundary conditions for (16) also need to be given on the 7-cm variability contour:

$$\overline{\eta}_{\text{bound}} = \overline{\eta}_{\text{Lev}} \qquad |_{\text{variability}=7\text{ cm}} \tag{17}$$

So at the boundaries we prescribed $\overline{\eta}$ derived from the *Levitus* [1982] climatology. Following this two-step approach the mean sea surface dynamic topography, $\overline{\eta}$, can be estimated as a function of the horizontal coordinates x and y. To find $\overline{\eta}$ that fulfills both equations (11)-(13) and (10) the above-described procedure has

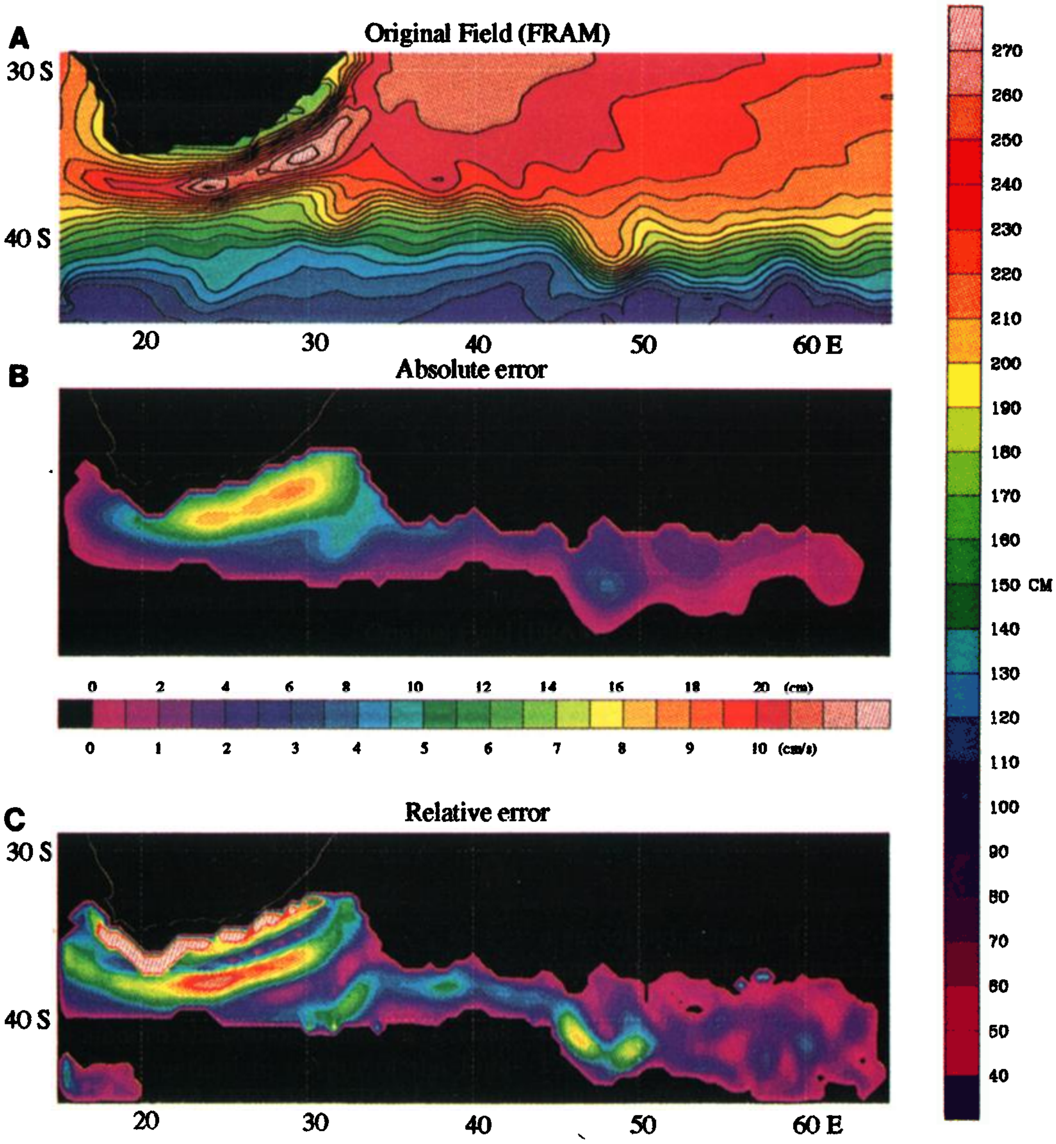

Plate 5. (a) Original 2-year averaged FRAM dynamic topography. (b) Absolute error defined as the difference between the best solution and the original dynamic topography. (c) Relative error defined as $\sqrt{u^2 + v^2}$, where u and v are the geostrophic surface velocities derived from the absolute error in the dynamic topography.

to be repeated by computing a new $\overline{u}_*$, $\overline{v}_*$, $\partial\overline{\zeta_*}/\partial x$, and $\partial\overline{\zeta_*}/\partial y$ and following the same solving strategy. After each iteration the new $\overline{\eta}$ field is regarded as the new (improved) climatology until the solution has converged to an $\overline{\eta}$ field that in very good approximation fulfills (10).

3.3. Testing the Method

To test the applicability of the proposed method for improving the smooth climatology (such as *Levitus* [1982]), we applied the method to output of the Fine Resolution Antarctic Model (FRAM) [FRAM group, 1991]. Several earlier studies have shown that FRAM results compare with altimeter data [e.g., *Feron*, 1995; *Lutjeharms and Webb*, 1995]. The results of such an eddy-resolving model supply a perfect test for control purposes. Two years of FRAM surface pressure fields have been used to derive eddy statistics, namely the divergence of the average eddy fluxes of relative vorticity. Exactly the same techniques were used as those used for computing the eddy statistics from Geosat data. Taking a smoothed version of the 2-year averaged FRAM dynamic topography as initial field (Plate 4a), the solution strategy as described above is applied to the Agulhas Current Region. Plates 4a-4c show the smoothed initial FRAM field, the FRAM eddy divergence, and the final solution after applying the method, respectively. Plate 5 shows the original FRAM field together with the absolute and relative error. The absolute error is defined as the difference between the original field and the best solution. The relative error is defined as $\sqrt{u^2 + v^2}$, where

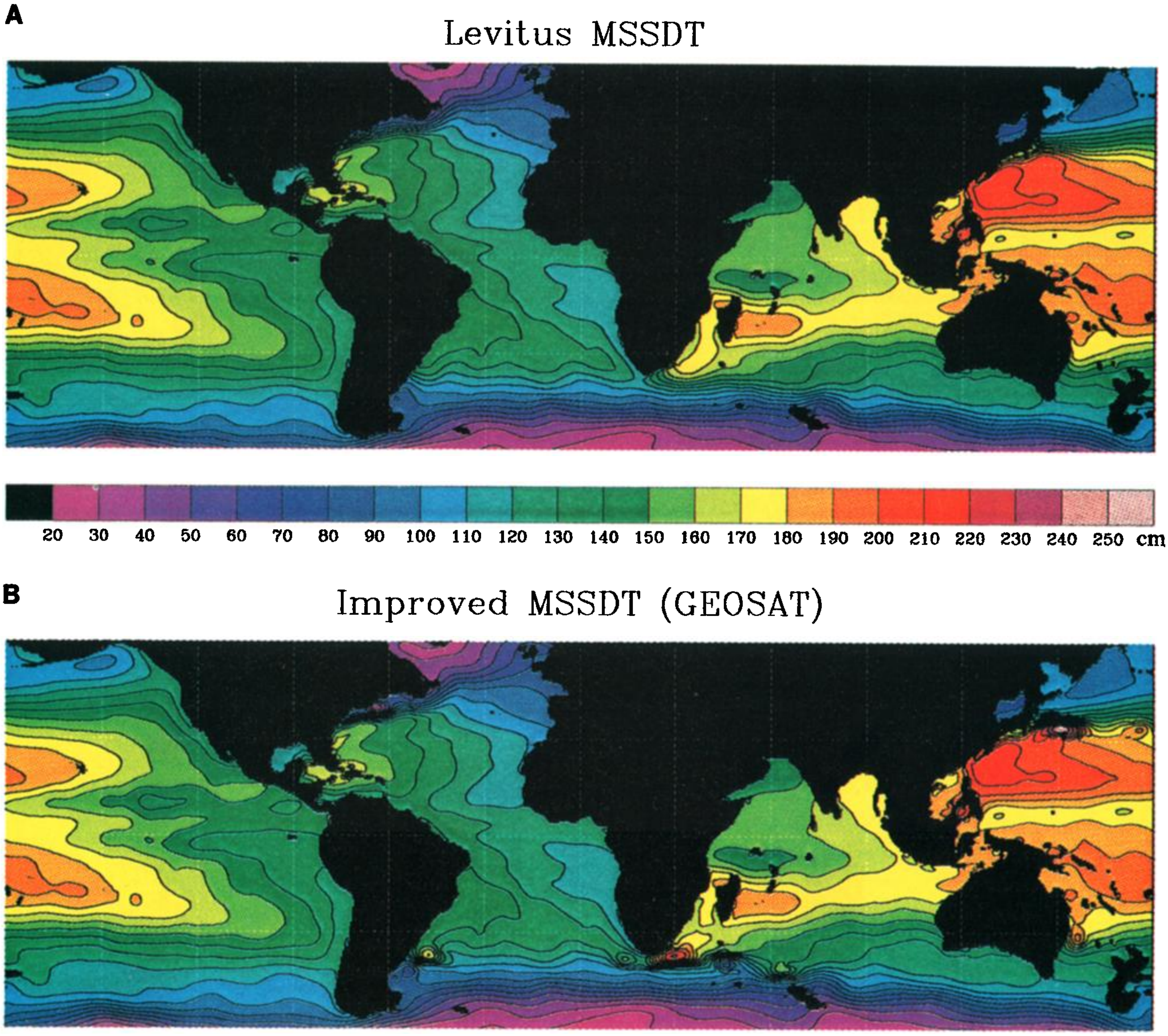

Plate 6. (a) The MSSDT from Levitus relative to 1000 dbar. (b) New MSSDT solution from the potential vorticity approach. Differences only occur in ocean areas with strong variability, i.e., the western boundary currents.

u and v are the geostrophic surface velocities derived from the absolute error in the solution.

3.4. Measurement Error Propagation

An error of 0.05 m in the altimeter observations of η' will be propagated to the surface velocity fields u' and v'; eddy stress terms $\overline{u'u'}$, $\overline{v'v'}$, and $\overline{u'v'}$; and mean relative vorticity eddy flux terms $\overline{u'\zeta'}$ and $\overline{v'\zeta'}$. Error propagation rules result in 0.07 m s^{-1} for u' and v'; 8.1×10^{-3} m^2 s^{-2} for $\overline{u'u'}$, $\overline{v'v'}$, and $\overline{u'v'}$; and 1.0×10^{-8} m s^{-2} for $\overline{u'\zeta'}$ and $\overline{v'\zeta'}$. These error propagation estimates are based on computing spatial derivatives over 1^o spatial distances at 45^o latitude. To get some insight in how these errors translate into errors in the final MSSDT, a sensitivity test was performed by using the solution strategy described in the previous section. From this test an upper bound of 8-10 cm could be derived for active ocean regions.

4. Application to Western Boundary Currents

In this section the iterative solving strategy described above for obtaining an approximate mean surface dynamic topography from the observed eddy fluxes is applied to the most eddy-active areas of the world ocean. After 30 iterations, where the new $\overline{\eta}$ is repeatedly used to derive a new $\overline{u}_*$ and $\overline{v}_*$ field, the solution converges to $\overline{\eta}$ as shown in Plate 6b. The climatologic field from *Levitus* [1982], which is used as boundary condition and initial field, is shown in Plate 6a.

In ocean regions where strong eddy activity is ob-

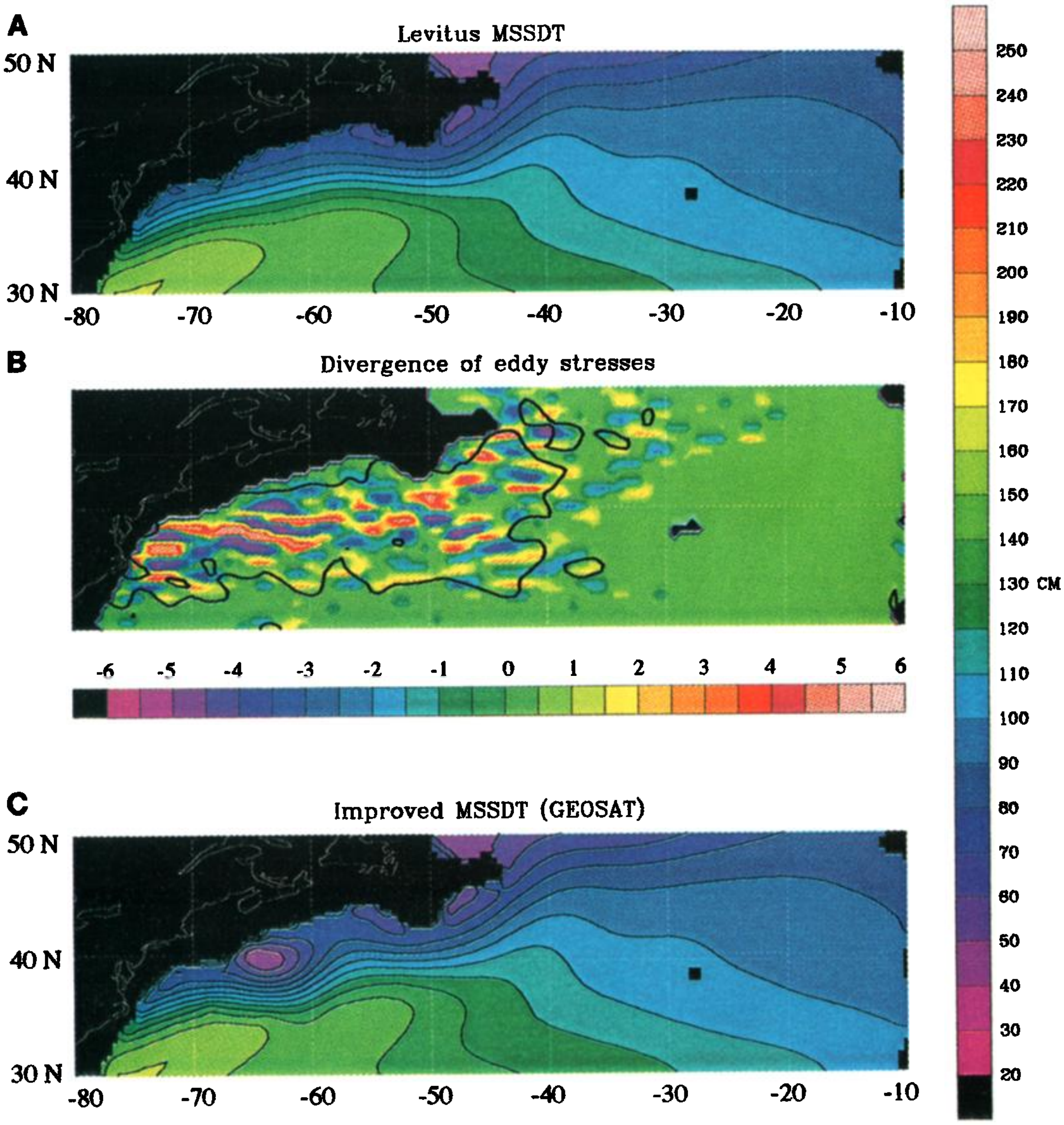

Plate 7. (a) The MSSDT in the Gulf Stream area in dynamic centimeters from the *Levitus*, [1982] climatology, relative to 1000 dbar. (b) The divergence of the eddy flux stress terms enlarged from the bottom panel of Plate 1 (units are $\times 10^{-13}$ s^{-2}); the 7-cm variability contour is shown on which the boundary conditions are prescribed. (c) New MSSDT solution from the conservation of potential vorticity approach (section 3); the contour interval is 10 cm.

served (Plates 1 and 2), the gradients in the solution for $\overline{\eta}$, corresponding to surface geostrophic velocities, are increased. In other ocean areas the eddy vorticity fluxes are too small (Plates 7b-11b), and the new solution is forced to and thus equivalent to the climatology. Those regions where the method applies correspond to the western boundary currents and their extensions and frontal areas in the Antarctic Circumpolar Current. The relevance of the new results (Plate 6b) compared to MSSDT fields determined from simultaneous approximation of the gravity field and the MSSDT is that they contain the total variety of spatial scales, from 200 km to the very large scales.

Because the method only applies for certain regions in the ocean, the major western boundary currents will be studied in more detail. To achieve better comparison between the climatology and the improved MSSDT fields, the Gulf Stream (GS), the Kuroshio Extension (KE), the Brazil/Malvinas Confluence (BMC), the Agulhas Extension (AE), and the East Australian Current (EAC) are shown separately and enlarged in Plates 7-11.

The Gulf Stream is probably the best investigated western boundary current of the world ocean [e.g., *Fofonoff*, 1981; *Watts*, 1983]. Gulf Stream meandering including warm and cold core ring formation has been

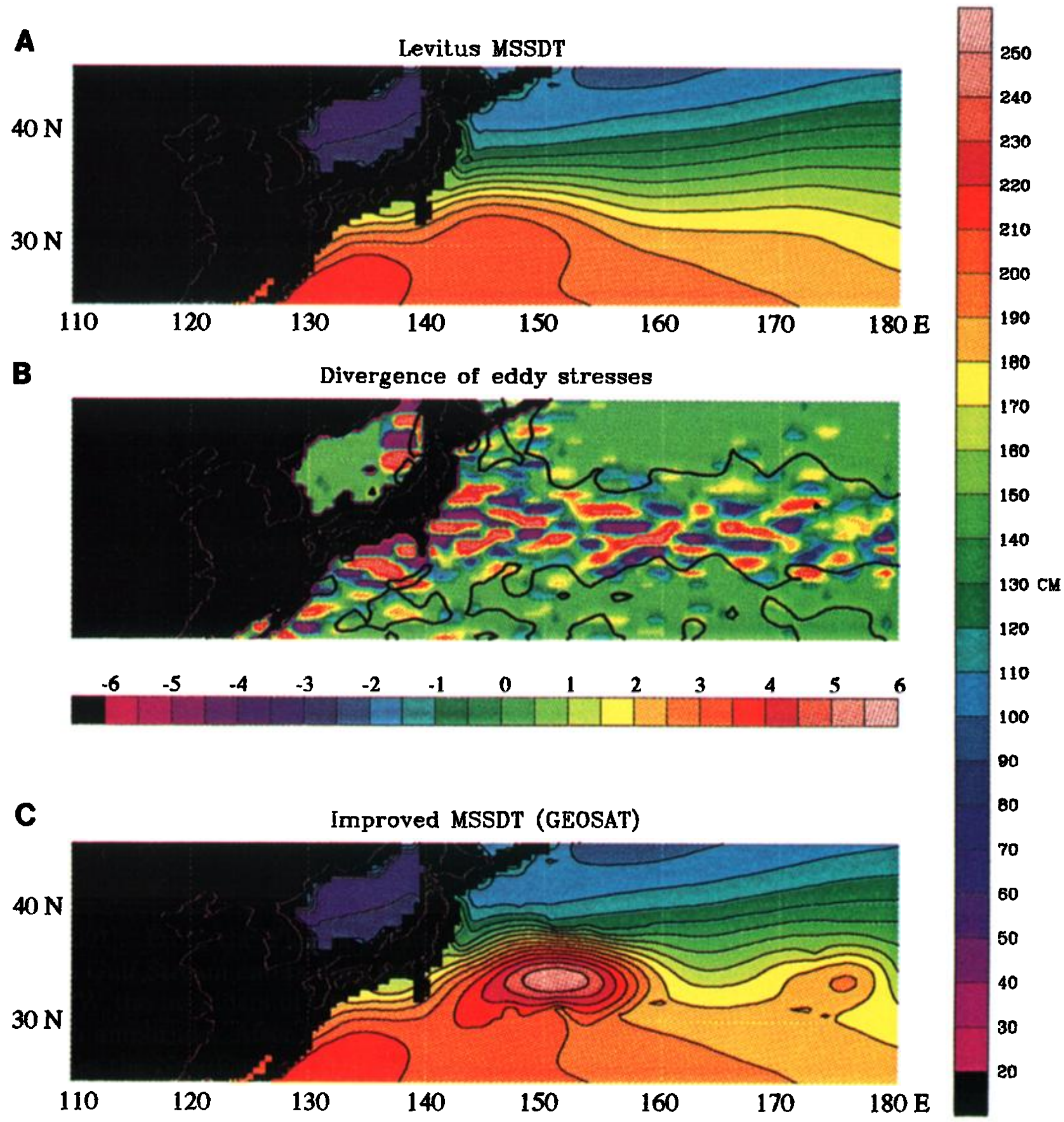

Plate 8. (a) The MSSDT in the Kuroshio Extension in dynamic centimeters from the *Levitus* [1982] climatology, relative to 1000 dbar. (b) The divergence of the eddy flux stress terms enlarged from the bottom panel of Plate 1 (units are $\times 10^{-13}$ s^{-2}); the 7-cm variability contour is shown on which the boundary conditions are prescribed. (c) New MSSDT solution from the conservation of potential vorticity approach (section 3); the contour interval is 10 cm.

studied extensively by hydrography, drifters, satellite imagery, and altimeter observations of the sea surface [e.g., *Olson et al.*, 1983; *Halliwell and Mooers*, 1983; *Maul et al.*, 1978; *Cornillon*, 1985; *Kelly and Gille*, 1990; *Zlotnicki*, 1991]. From the Florida Straits past Cape Hatteras the Gulf Stream enters deep waters. At approximately 70°W the meanders of the Gulf Stream start to increase in amplitude. After 62°W, where the Gulf Stream reaches the New England Seamounts, the meandering continues to increase. Figure 1a shows the 1-year mean position of the Gulf Stream as derived from a high-resolution quasi-geostrophic numerical model which has been assimilated with TOPEX/POSEIDON altimeter data (for more details, see *Blayo et al.* [1994]). The Gulf Stream path seems to be stationary until the current reaches 65°W, whereafter the standard deviation (Figure 1a) increases significantly. This indicates an north-south increase of the envelope of Gulf Stream positions. These model results somewhat contradict a study of *Cornillon* [1985], who found from satellite temperature images that the envelope which constrains the Gulf Stream positions did not increase between 68° and 58°W. Relevant for our study is that the cross-frontal length scale of the envelope defines how strong the instantaneous Gulf Stream position will be smoothed by averaging over a long time interval. The new approximation for $\overline{\eta}$ (Plate 7c) shows a more or less zonal Gulf Stream from Cape Hatteras to 63°W. At this point the

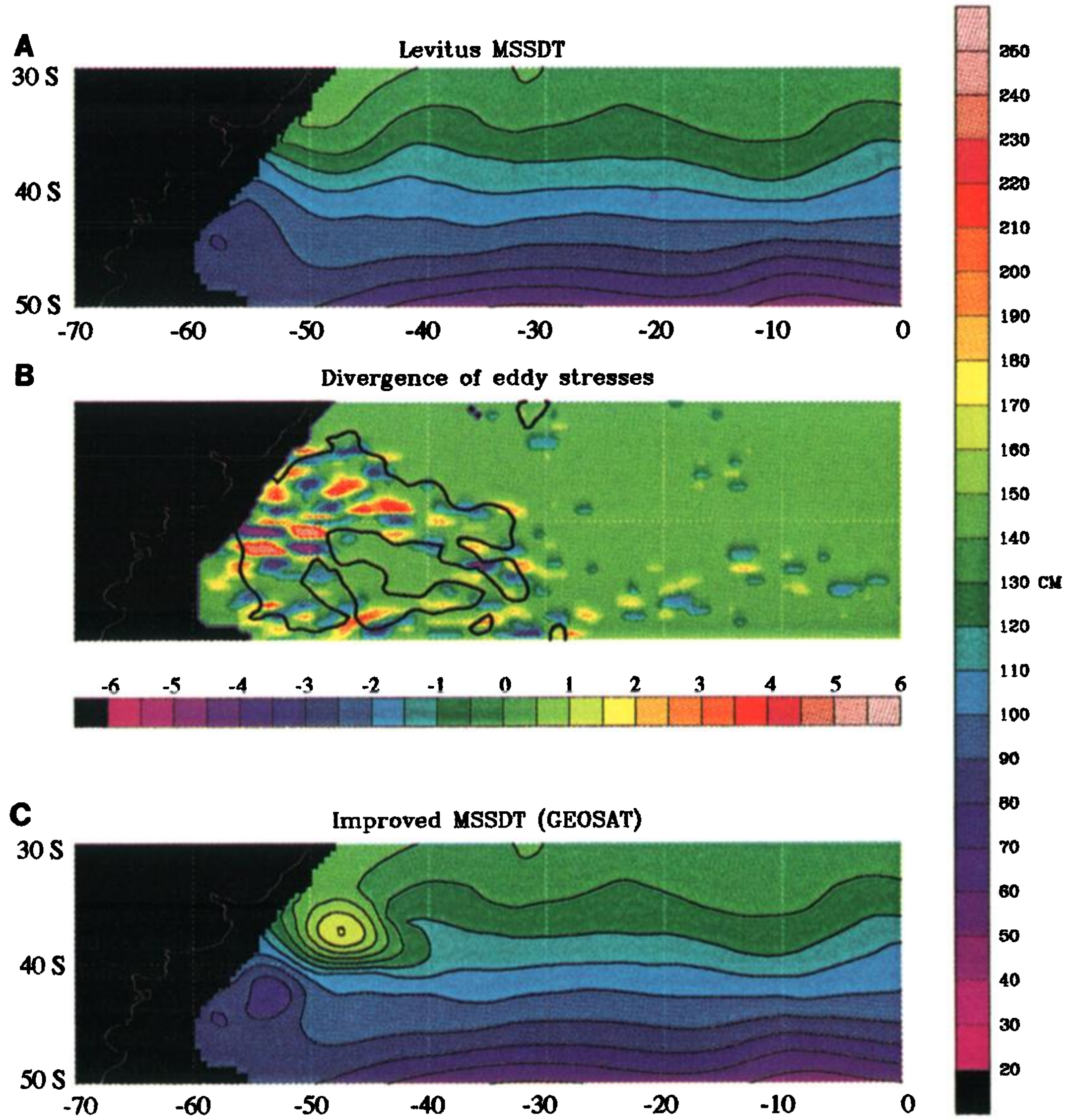

Plate 9. (a) The MSSDT in the Brazil/Malvinas Confluence in dynamic centimeters from the *Levitus* [1982] climatology, relative to 1000 dbar. (b) The divergence of the eddy flux stress terms enlarged from the bottom panel of Plate 1 (units are $\times 10^{-13}$ s^{-2}); the 7-cm variability contour is shown on which the boundary conditions are prescribed. (c) New MSSDT solution from the conservation of potential vorticity approach (section 3), the contour interval is 10 cm.

mean Gulf Stream bends a few hundred kilometers to the north whereafter it follows a zonal path to the east along the 40°N latitude band. This Gulf Stream pattern is in remarkable good agreement with the findings of recent other studies designed to determine the mean Gulf Stream position [e.g., *Kelly and Gille*, 1990; *Glenn et al.*, 1991; *Blayo et al.*, 1994] (Figure 1a).

The Kuroshio Current separates the southern coast of Japan at 140°E and 35°N. After separation it is named the Kuroshio Extension, which is characterized, as the Gulf Stream east of approximately 70°W, as an eastward flowing inertial jet with large amplitude meanders and warm and cold core ring formations. Mesoscale perturbations generally propagate westward [e.g., *Tai and White*, 1990; *Qiu et al.*, 1991]. Annual and interannual variability appears to be a prominent element of the KE and was found in temperature data [e.g., *Mizuno and White*, 1983], direct current measurements accompanied with hydrographic observations [e.g., *Schmitz et al.*, 1987] and satellite altimeter data [e.g., *Tai and White*, 1988; *Qiu et al.*, 1991]. Figure 1b shows the Kuroshio mean position derived from 2.5 years of Geosat altimeter data. The position is digitized from *Qui et al.* [1991], who fitted a synthetic current's height profile to independent satellite tracks. The Kuroshio Extension differs from the other western boundary currents in the sense that it has two modes between which the Kuroshio can switch, one with a

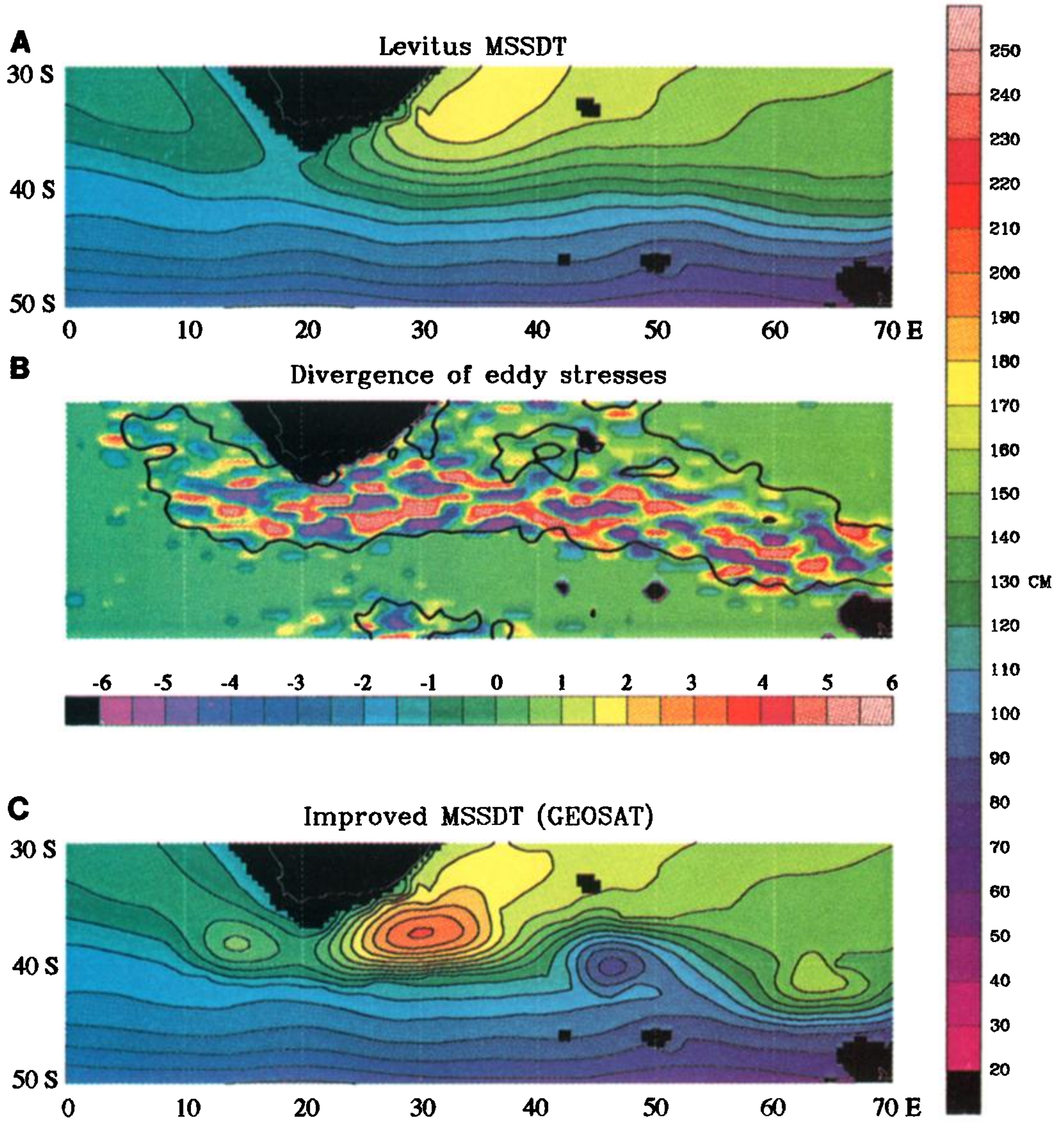

Plate 10. (a) The MSSDT in the Agulhas Extension in dynamic centimeters from the *Levitus* [1982] climatology, relative to 1000 dbar. (b) The divergence of the eddy flux stress terms enlarged from the bottom panel of Plate 1 (units are $\times 10^{-13}$ s^{-2}); the 7-cm variability contour is shown on which the boundary conditions are prescribed. (c) New MSSDT solution from the conservation of potential vorticity approach (section 3); the contour interval is 10 cm.

more northern trajectory than the other. This bimodality diffuses the definition of a long-term mean current position; that is, the climatology will be a smoothed representation of the two Kuroshio modes. The new approximation for $\overline{\eta}$ (Plate 8c) reveals the Kuroshio Extension has its maximum northward position at approximately 150°E, whereafter is slightly turns to the south. Surface currents are clearly enhanced compared to the Levitus climatology.

In the Brazil/Malvinas Confluence region the Brazil Current and the Malvinas Current converge and form a strong thermal front which has been observed between 38° and 46°S [e.g., *Legeckis and Gordon*, 1982; *Olson et al.*, 1988; *Gordon*, 1989; *Confluence Principal Investigators*, 1990]. An example of hydrographic observations from the Brazil/Malvinas Confluence can be found in Figure 1e. The new approximation (Plate 9c) for $\overline{\eta}$ reveals a well defined confluence position between 39° and 42°S with a quasi-stationary wave-like pattern. It compares well with results found in hydrographic observations for Brazil Current extension [e.g., *Confluence Principal Investigators*, 1990]. The wave-like pattern seems a realistic phenomenon and is also observed in other western boundary regions. Comparing the *Levitus* [1982] climatology (Plate 9a) with the new approximation (Plate 9c) shows the increase of horizontal resolution in the MSSDT field.

When the Agulhas Current runs out of western

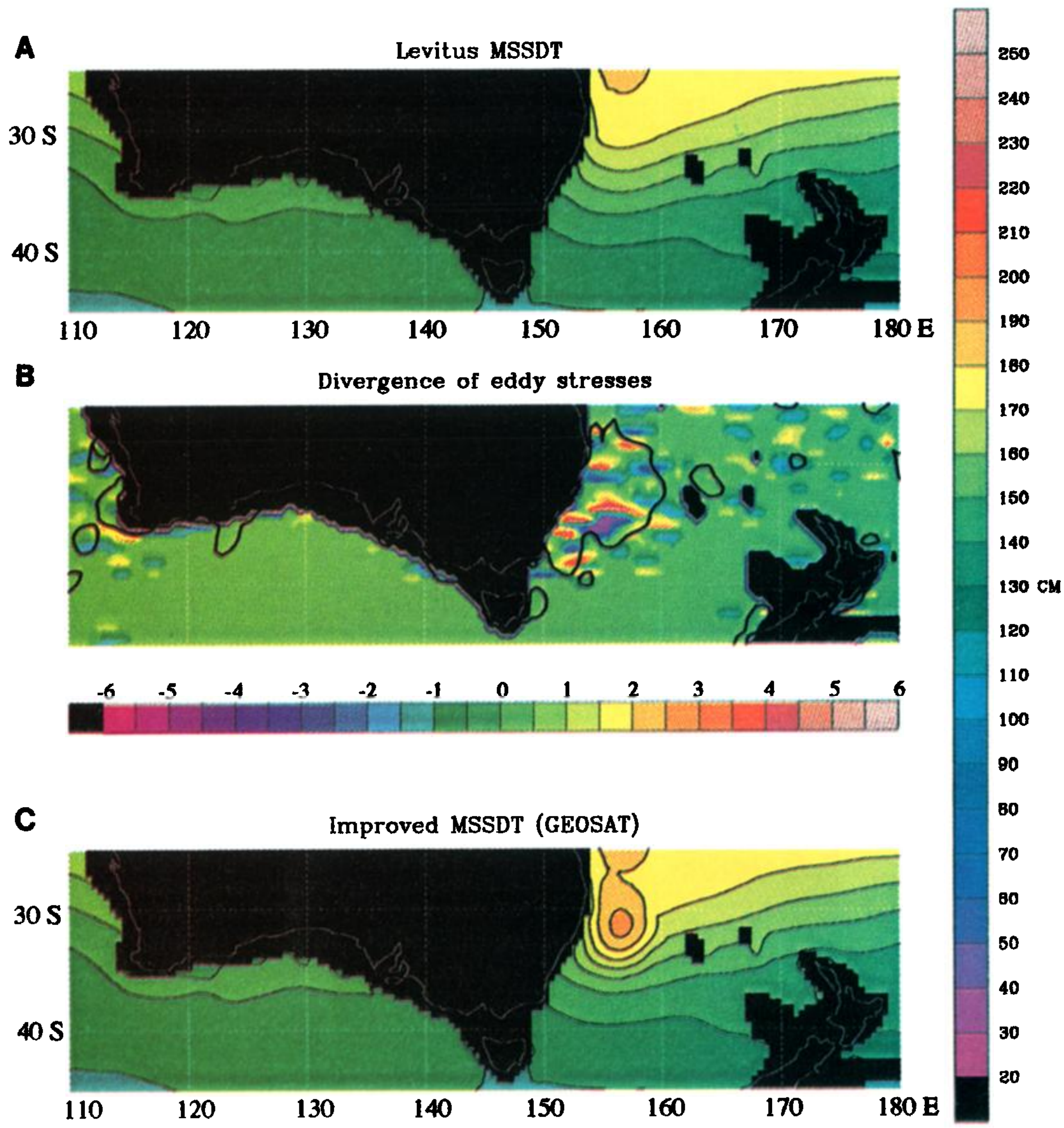

Plate 11. (a) The MSSDT in the East Australian Current in dynamic centimeters from the *Levitus* [1982] climatology, relative to1000 dbar. (b) The divergence of the eddy flux stress terms enlarged from the bottom panel of Plate 1 (units are $\times 10^{-13}$ s^{-2}); the 7-cm variability contour is shown on which the boundary conditions are prescribed. (c) New solution from the conservation of potential vorticity approach (section 3), the contour interval is 10 cm.

boundary, it separates and makes a large almost 180° anticyclonic turn which is generally referred to as the Agulhas Retroflection [e.g., *Ou and De Ruijter*, 1986; *Boudra and Chassignet*, 1988; *Lutjeharms and van Ballegooyen*, 1988]. The Agulhas Return Current carries most of the Agulhas water back into the Indian Ocean (see Figure 1c). In the Agulhas Extension the new approximation for $\overline{\eta}$ reveals a more intense westward penetration of the Agulhas Current (Plate 10c) in the region where it retroflects [e.g., *Harris et al.*, 1978; *Gordon et al.*, 1987; *Lutjeharms and van Ballegooyen*, 1988]. The Agulhas Retroflection, which is totally absent in the Levitus climatologic fields, is clearly present in the new solution between 20° and 25°E. This position for the Agulhas Retroflection is also observed in hydrographic measurements from the Agulhas Current (compare Figure 1c). Also, the path of the Agulhas Current is clearly visible. Some evidence for a large meander (wave-like pattern which may be related to bottom topography) in the Agulhas Extension downstream from the retroflection can be observed in Plate 10c.

The East Australian Current (Plate 11) is a relatively weak surface current. It flows southward along the continental slope and usually separates from the coast between 31° and 33°S and forms a large anticyclonic meander which may extend southward as far as 38°S [e.g., *Mulhearn*, 1987] (see Figure 1d). The new approximation evidently has more structure in the time-averaged flow pattern. The results shown in Plate 11c agree with the most likely position of the East Australian Current

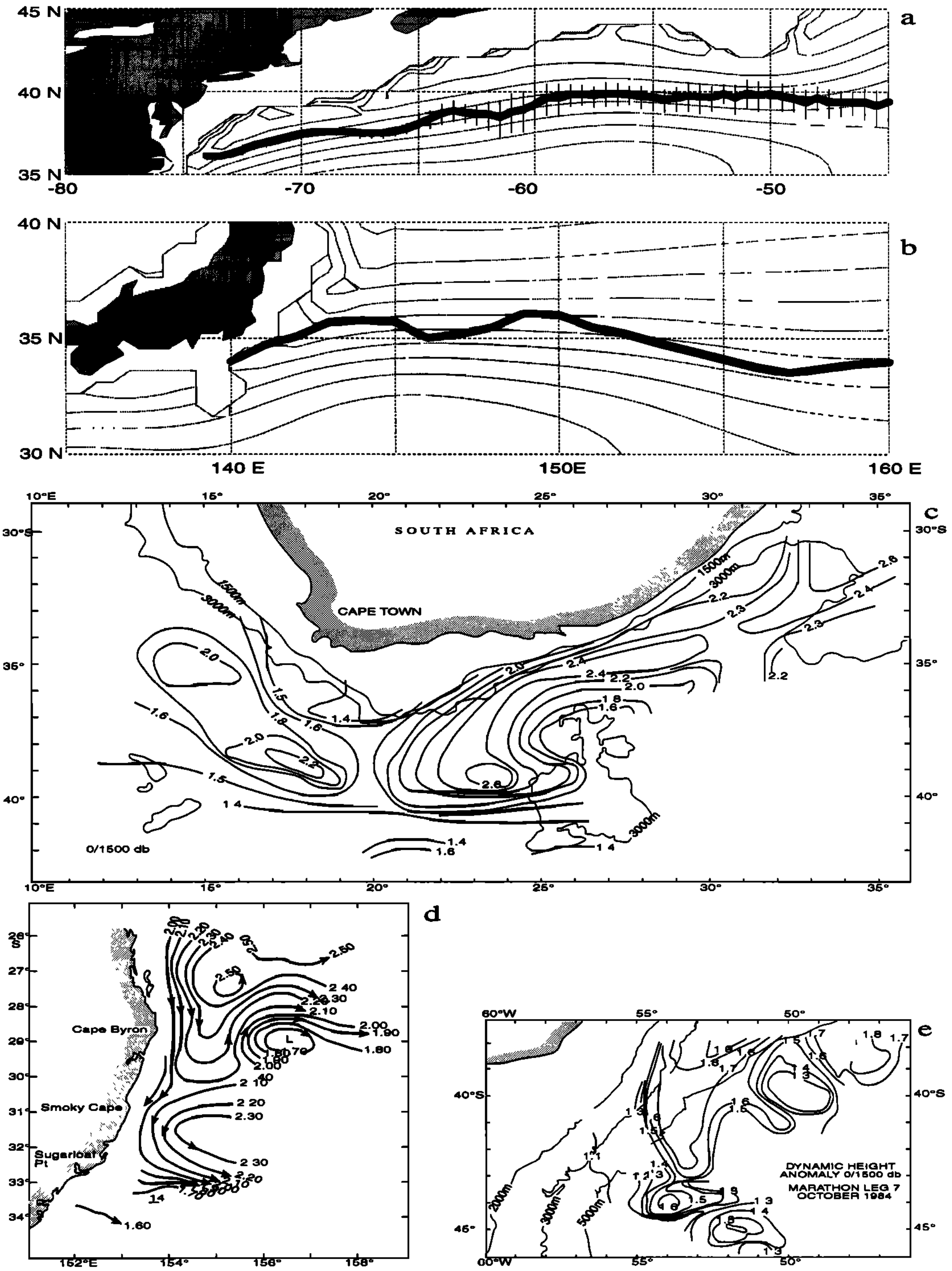

Figure 1. (a) Gulf Stream climatology [*Levitus*, 1982] with its mean position (thick line), derived from a high-resolution quasi-geostrophic model which has been assimilated with TOPEX/POSEIDON data, superimposed. (b) Kuroshio Current climatology [*Levitus*, 1982] with its mean position (thick line), derived by fitting a synthetic Gaussian-shaped velocity profile though 2.5 years of Geosat altimeter data (digitized from *Qiu et al.* [1991]), superimposed. (c) The sea surface dynamic topography in the Agulhas Current relative to the 1500-dbar surface [after *Gordon et al.*, 1987]. (d) The sea surface dynamic topography in the East Australian Current relative to the 1300-dbar surface [after *Boland and Church*, 1981]. (e) The sea surface dynamic topography in the Brazil/Malvinas Confluence relative to the 1500-dbar surface [after *Gordon*, 1989]. All heights are given in dynamic meters

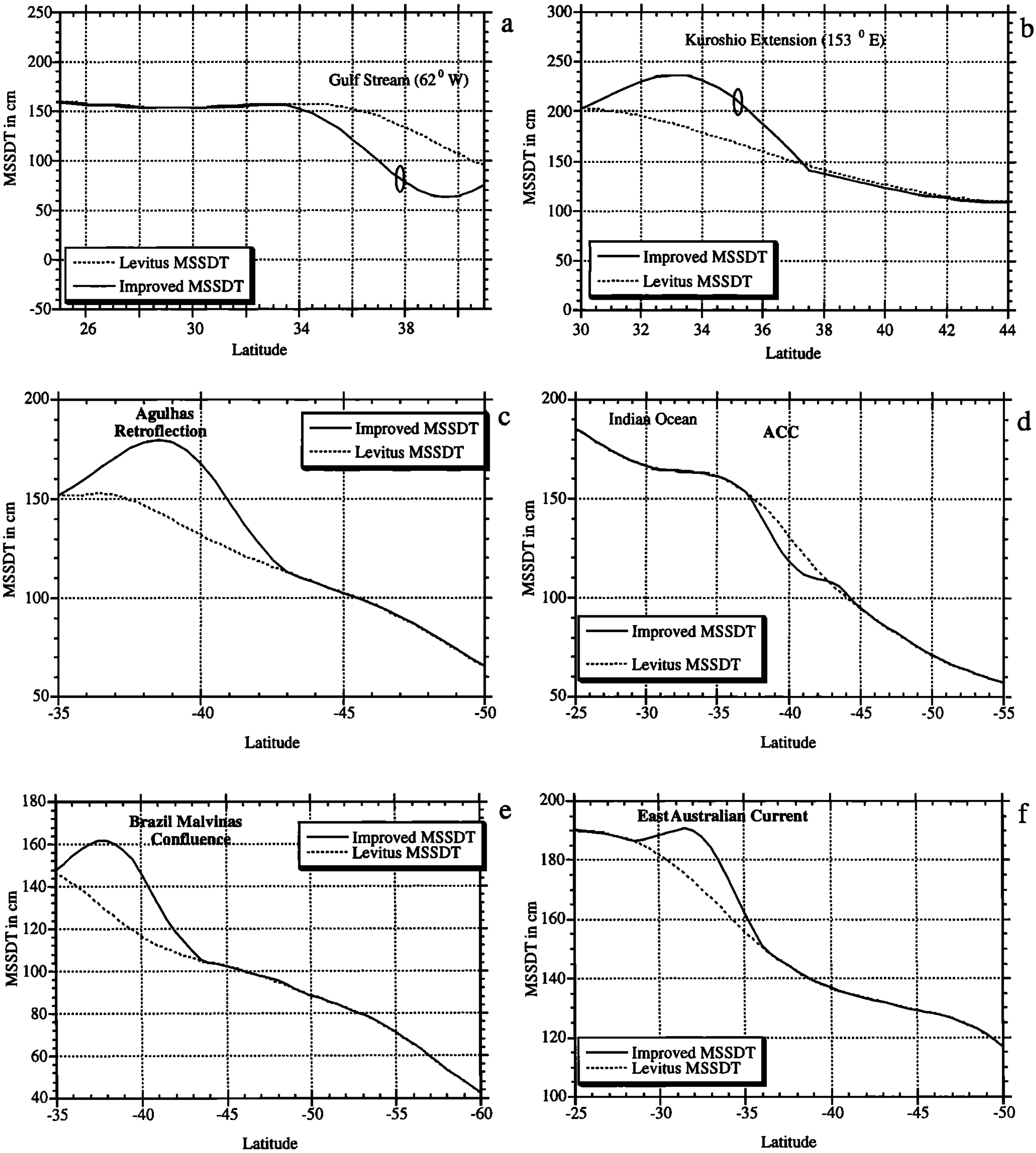

Figure 2. Meridional section of (a) the Gulf Stream MSSDT at 62.0°W and (b) of the Kuroshio Extension at 153.0°E. The dashed and solid lines show the *Levitus* [1982] climatology and the new solution from the potential vorticity approach (section 3), respectively. Meridional section of the Agulhas Current system (c) at 24.5°E and (d) at 54.5°E. (e) Meridional section of the Brazil/Malvinas Confluence at 50.0°W. (f) Meridional section of the East Australian Current at 157.5°E.

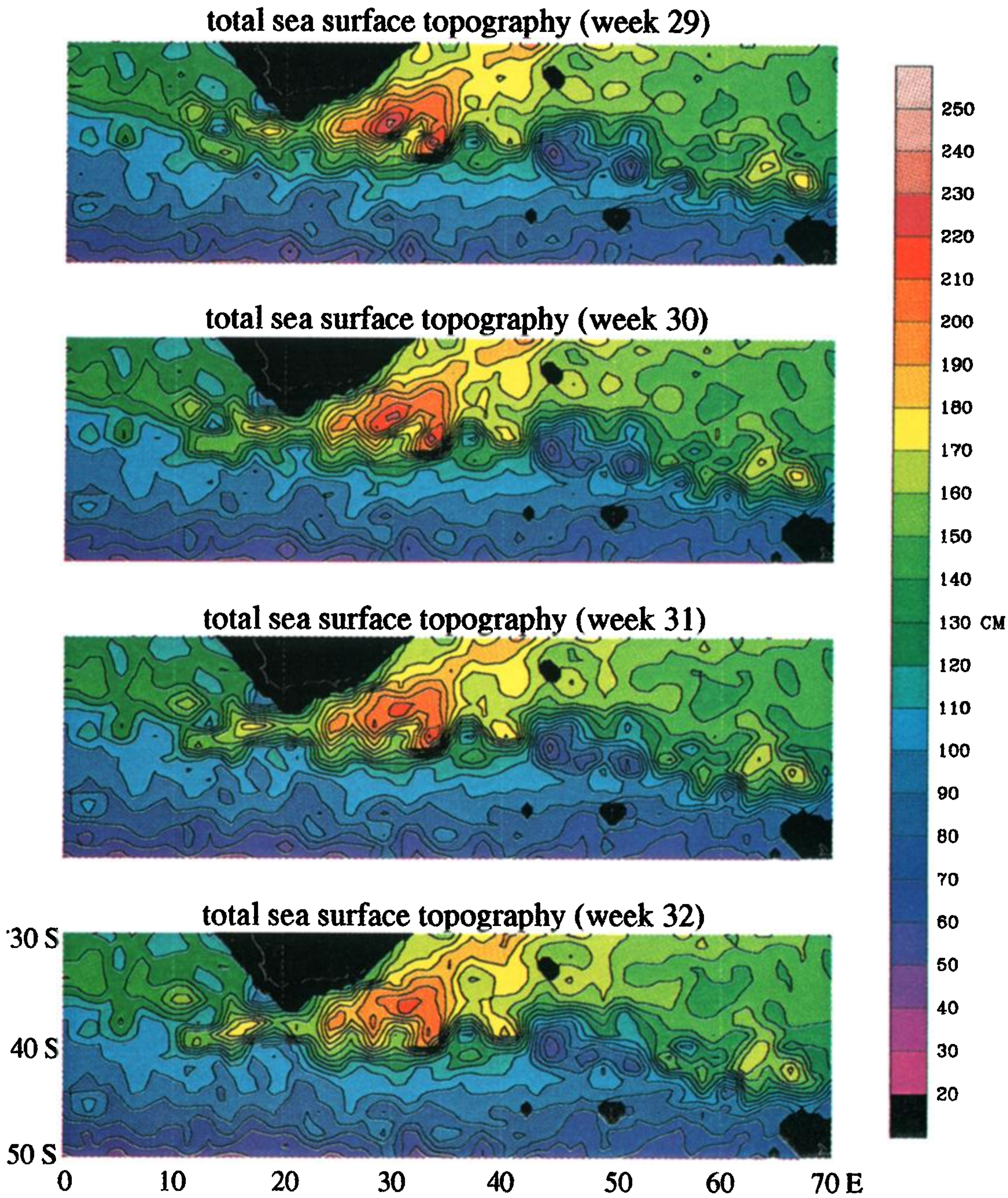

Plate 12. A time sequence of the absolute dynamic height in the Agulhas Retroflection at weekly intervals determined by applying the proposed method to Geosat altimeter height observations. Ring shedding can be observed. Analysis of the 3-year observational period shows that 12 similar ring-shedding events occurred. Time is relative to November 8, 1986, and the contour interval is 10 cm.

derived from satellite infrared imagery [*Mulhearn*, 1987] and hydrography [*Boland and Church*, 1981].

5. Meridional Cross Sections

A more detailed comparison can be made between climatology and the improved MSSDT fields by analyzing meridional sections of dynamic topography. For this purpose, six sections were chosen, one each in the Gulf Stream and the Kuroshio Extension, two in the Agulhas Extension, and one each in the Brazil/Malvinas Confluence and East Australian Current (Figure 2). The new MSSDT fields are calculated over the total ERM period of Geosat (from November 1986 to September 1989).

The meridional section in the Gulf Stream is chosen at 62°W (Figure 2a). The mean Gulf Stream latitude derived from *Blayo et al.* [1994] is marked in the plot, which is the position where the MSSDT gradient has its maximum.

Figure 2b shows the meridional section though the Kuroshio Extension at 153°W. The mean Kuroshio latitude from *Qiu et al.* [1991] is marked in the plot. The new MSSDT solution suggests a slightly more northward front position.

In the cross section at 24.5°E which is right through the Agulhas Retroflection (Figure 2c) the new method shows a realistic more westward penetration of the Agulhas Current which is not present in the Levitus climatology.

Improvements in the MSSDT at the 54.5°E section shown in Figure 2d are clearly confined to the Antarctic Circumpolar Current, roughly between 37° and 44°S. The north-south gradient of the heights is increased with an approximate factor of 2. Maximum surface geostrophic velocity is 8 cm/s and 20 cm/s in the climatology and new solution, respectively. Such a result could be expected as the Levitus climatology is a mean over unevenly distributed samples and spread over more than 50 years in time. Climatology over the much shorter Geosat period determined by our method should lead to sharper mean jets, given the (in situ) observed jet like nature of the ACC in this area [e.g., *Olbers et al.*, 1992].

Compared to the Levitus climatology the center of the ACC (or its front) is shifted to the north by approximately 100 km. This is also observed in spatial fields of the MSSDT (Plate 10).

The meridional section in the BMC is chosen at 50.0°W (Figure 2e). In the improved MSSDT the Brazil/Malvinas Extension is located at approximately 40°-42°S, which is in agreement with hydrographic data [e.g., *Confluence Principal Investigators*, 1990]. Translated into surface geostrophic flow the climatology of 7 cm/s is increased to 15 cm/s for the potential vorticity approach (Figure 2e).

Figure 2f shows the section through the EAC which is chosen at 157.5°E. The current is located between 32° and 34°S with a surface geostrophic velocity of 11 cm/s. Climatology gives a surface velocity of only 5 cm/s. The results compare well with the average position of the Tasman Front, derived by *Mulhearn* [1987], from satellite thermal imagery between 1982 and 1985.

6. Combining Mean and Time-Varying Flow Fields: With Application to Agulhas Ring Shedding

Adding the computed MSSDT to the observed relative sea heights gives absolute dynamic sea surface heights at every desired time. A very striking application can be shown the Agulhas Current Retroflection region. Plate 12 shows a time sequence of sea surface heights in the Agulhas Retroflection. It reveals the formation of a large Agulhas ring. From applying our method to the 3-year Geosat observational period in the Agulhas Retroflection, 12 major ring-shedding events could be determined of which Plate 12 shows one example. These shedding events correspond to the dominant EOF modes as analyzed by *Feron et al.*, [1992]. Besides 12 ring-shedding events the following picture of what happens in the Agulhas Retroflection emerges: The Agulhas Current occasionally interacts with recently formed rings. Over the 3-year observational period this strong interaction resulted in several reabsorption events (we counted six of them) which means that one ring is in fact shedded twice. Also, smaller rings are occasionally formed. The observed translation speed of large Agulhas rings is typically 8 cm/s just after separation. Their characteristic spatial scale is approximately 300 km.

7. Summary and Discussion

In this study we proposed, applied, and analyzed a simple method to improve the smooth climatologic mean sea surface dynamic topography with satellite altimeter observations. We have shown that in areas with large eddy variability, vorticity input by the wind and stretching are small compared to the divergence of the relative vorticity stress and advection of relative and planetary vorticity. Starting from a simplified vorticity equation, we have presented a method to better approximate the time-averaged flow field in areas with large enough mesoscale variability. The model includes divergence of the relative vorticity stress (measured by altimeter), advection of relative vorticity, and advection of planetary vorticity. The proposed method only applies to ocean regions with strong mean currents and sufficient temporal variability such as the major western boundary currents and their extensions.

Application of the method to the five major western boundary current systems, the Gulf Stream, the Kuroshio Current, the Agulhas Current, the Brazil/Malvinas Confluence, and the East Australian Current, shows promising results. The new results contain the total variety of spatial scales, from 200 km to the very large scales. On average the new solution results in geostrophic surface currents which are more narrow and a factor of 2 stronger than Levitus climatology. To what degree the new results are affected by the boundary conditions taken from the climatology, which includes the assumption of a level of no motion, is under investigation.

Application of the method to the Agulhas Current retroflection region revealed for the first time a full sequence of actual ring-shedding events over the Geosat period. So far, the lack of a mean current field precluded such an analysis (e.g., Plate 12). It revealed that rings are regularly reabsorbed and then shed again. Over the period from November 1986 to September 1989 a net amount of 12 Agulhas rings was pinched off, which is 30% less than earlier estimates [*Gordon and Haxby*, 1990; *Feron et al.*, 1992].

The purpose of the present study was to investigate whether the simplified vorticity equation could be used to obtain reasonable and possibly surprising results in large parts of the Southern Ocean. By comparing the result with hydrographic observations we conclude that indeed the vorticity-based method gives realistic results. Moreover, the method was tested by applying it to output of the United Kingdom Fine Resolution Antarctic Model [*FRAM Group*, 1991].

In this study, eddy stresses have been determined by averaging over 3 years, i.e., the complete Geosat Exact Repeat Mission data set. If averaging over, say, 1 year would be sufficient to determine eddy stresses accurately, for every separate year a MSSDT can be determined. Then it allows the investigation of interannual (long-term) changes in the flow field. Furthermore, using the same method with TOPEX/POSEIDON observations will give insight in the solution's sensitivity to the eddy stress terms derived by different satellites averaged over different years.

Given a density profile, geostrophic velocities may now be computed at every depth. The classic problem of assuming a level of no motion, at great depth, may therefore be no longer necessary. The new MSSDT improves the difficult interpretation of sea level anomalies alone. The exchange and redistribution of momentum and energy between eddies and the mean flow may be studied in detail (Plate 12). Fluxes and transports across the Antarctic Circumpolar Current (of which the mean position is determined by this method) may be estimated particularly if the surface fields are coupled to a diagnostic, multilayer, eddy-resolving numerical model.

The expected accuracy of the marine geoid at scales shorter than about 1400 km is not adequate for determination of the mean global ocean circulation at these length scales [*Chelton*, 1988; *Nerem et al.*, 1990]. The only direct way to use satellite altimeter observations for determining the mean global ocean circulation is to combine the altimeter observations with a geoid model with centimeter precision at all wavelengths. Thus, as long as there is no accurate geoid down to the mesoscale, the results presented in this study may be a good alternative.

Acknowledgments. We like to thank Roger Haagmans for preprocessing the altimeter data at Delft University of Technology. This investigation was partly funded by the Space Research Organization Netherlands (SRON) and NOPII.

References

Blayo, E., J. Verron, J.M. Molines, Assimilation of TOPEX/POSEIDON altimeter data into a circulation model of the North Atlantic, *J. Geophys. Res.*, *99*, 24691–24705, 1994.

Boland, F.M., and J.A. Church, The East Australian Current 1978, *Deep Sea Res., Part A, 28*, 937–957, 1981.

Boudra, D.B., and E.P. Chassignet, Dynamics of Agulhas retroflection and ring formation in a numerical model, 1, The vorticity balance, *J. Phys. Oceanogr.*, *18*, 280–303, 1988.

Chelton, D.B., WOCE/NASA altimeter algorithm workshop, *U.S. WOCE Tech. Rep. 2*, 70 pp., U.S. Planning Off. for WOCE, College Station, Tex., 1988.

Cheney, R.E., J.G. Marsh, and B.D. Beckley, Global mesoscale variability from collinear tracks of SEASAT altimeter data, *J. Geophys. Res.*, *88*, 4343–4354, 1983.

Confluence Principal Investigators, CONFLUENCE 1988–1990: An intensive study of the Southwestern Atlantic, *Eos Trans. AGU*, *71*(41), 1131–1133, 1137, 1990.

Cornillon, P., The effect of the New England Seamounts on Gulf Stream meandering as observed from satellite IR imagery, *J. Phys. Oceanogr.*, *16*, 386–389, 1985.

Engelis, T., and P. Knudsen, Orbit improvement and determination of the ocean geoid and topography from 17 days of SEASAT data, Dep. of Geod. Sci. and Surv., Ohio State Univ., Columbus, 1989.

Feron, R.C.V., The Southern Ocean western boundary currents: Comparison of Fine Resolution Antarctic Model results with Geosat-altimeter data, *J. Geophys. Res.*, *100*, 4959–4975, 1995.

Feron, R.C.V., W.P.M. De Ruijter, and D. Oskam, Ring-shedding in the Agulhas Current System, *J. Geophys. Res.*, *97*, 9467–9477, 1992.

Fine Resolution Antarctic Model (FRAM) Group, An eddy-resolving model of the Southern Ocean, *Eos Trans. AGU*, *72*(15), 169, 174-175, 1991.

Fofonoff, N.P., The Gulf Stream system, in *Evolution of Physical Oceanography*, edited by B.A. Warren and C. Wunsch,., pp. 112–139, MIT press, Cambridge, 1981.

Fu, L-L., C.J. Koblinsky, J-F. Minster, and J. Picaut, Reflecting on the first three years of TOPEX/POSEIDON, *Eos Trans. AGU*, *77*(12), 109, 111, 117, 1996.

Gille, S.T., Mean sea surface height of the Antarctic Circumpolar Current from Geosat data: Method and application, *J. Geophys. Res.*, *99*, 18,255–18,273, 1994.

Glenn, S.M., D.L. Porter, and A.R. Robinson, A synthethic Geoid validation of Geosat mesoscale dynamic topography in the Gulf Stream region, *J. Geophys. Res.*, *96*, 7145–7166, 1991.

Gordon, A.L., Brazil/Malvinas Confluence-1984, *Deep Sea Res., Part A, 36*, 359–384, 1989.

Gordon, A.L., and W.F. Haxby, Agulhas eddies invade the South Atlantic: Evidence from Geosat altimeter and shipboard conductivity-temperature-depth survey, *J. Geophys. Res.*, *95*, 3117–3125, 1990.

Gordon, A.L.,J.R.E. Lutjeharms, and M.L. Gründlingh, Stratification and circulation at the Agulhas Retroflection, *Deep Sea Res., Part A, 34*, 565–599, 1987.

Halliwell, G.R., Jr., and C.N.K. Mooers, Meanders in the Gulf Stream downstream of Cape Hatteras, 1975–1978, *J. Phys. Oceanogr.*, *13*, 1275–1292, 1983.

Harris, T.F.W., R. Legeckis, and D. Van Forest, Satellite infra-red images in the Agulhas Current System, *Deep Sea Res.*, *25*, 543–548, 1978.

Hellermann, S., and M. Rosenstein, Normal wind stress over the world ocean with error estimates, *J. Geophys. Res.*, *13*, 1093–1104, 1983.

Holloway, G., and S.S. Kristmannsson, Stirring and transport of tracer fields by geostrophic turbulence, *J. Fluid Mech*, *141*, 27–50, 1984.

Holopainen, E.O., On the dynamic forcing of the long-term mean flow by the large-scale Reynolds stresses in the atmosphere, *J. Atmos. Sci.*, *35*, 1596–1604, 1978.

Hoskins, B.J., I.N. James, and G.H. White, The shape, propagation and mean-flow interaction of large-scale weather systems, *J. Atmos. Sci.*, *40*, 1595–1612, 1983.

Ichikawa, K., and S. Imawaki, Life history of a cyclonic ring detached from the Kuroshio Extension as seen by the Geosat altimeter, *J. Geophys. Res.*, *99*, 15,953–15,966, 1994.

Kelly, K.A., and S.T. Gille, Gulf Stream surface transport and statistics at 69°W from the Geosat altimeter, *J. Geophys. Res.*, *95*, 3149–3161, 1990.

Kelly, K.A., T.M. Joyce, D.M. Schubert, and M.J. Caruso, The mean sea surface height and geoid along the Geosat subtrack from Bermuda to Cape Cod, *J. Geophys. Res.*, *96*, 12,699–12,709, 1991.

Legeckis, R., and A. L. Gordon, Satellite observations of the Brazil and Falkland currents-1975 to 1976 and 1978, *Deep Sea Res.*, *Part A*, *29*, 275–401, 1982.

Levitus, S., Climatological atlas of the world ocean, *NOAA Prof. Pap. 13*, 173 pp., U.S. Dep. of Commer., 1982.

Lutjeharms, J.R.E., and R.C. van Ballegooyen, The retroflection of the Agulhas Current, *J. Phys. Oceanogr.*, *18*, 1570–1583, 1988.

Lutjeharms, J.R.E., and D.J. Webb, Modelling the Agulhas system with FRAM (Fine Resolution Antarctic Model), *Deep Sea Res.*, *Part 1*, *42*, 523–551, 1995.

Marsh, J.G., C.J. Koblinsky, F. Lerch, S.M. Klosko, J.W. Robbins, R.G. Williamson, and G.B. Patel, Dynamic sea surface topography, gravity, and improved orbit accuracies from direct evaluation of Seasat altimeter data, *J. Geophys. Res.*, *95*, 13,129–13,150, 1990.

Maul, G.A., P. Webb de Witt, A. Yanaway, and S.R. Baig, Geostationary satellite observations of Gulf Stream meanders: IR measurements and time series analysis, *J. Geophys. Res.*, *83*, 6123–6135, 1978.

Minster, J.F., C. Brossier, and P. Femenias, Global ocean dynamic topography and how it varies between October and December 1992, *AVISO Altimetry News.*, *2*, pp. 22–23, CNES, Toulouse, France, 1993.

Mizuno, K., and W.B. White, Annual and interannual variability in the Kuroshio Current system, *J. Phys. Oceanogr.*, *13*, 1847–1867, 1983.

Mulhearn, P.J., The Tasman front: A study using satellite infrared imagery, *J. Phys. Oceanogr.*, *17*, 1148–1155, 1987.

Naeije, M.C., E. Wisse, R. Scharroo, and K.F. Wakker, Ocean dynamics from the ERS-1 35-day repeat mission, in *Proceedings Second ERS-1 Symposium, Eur. Space Agency Spec. Publ.*, *ESA SP-361*, 501–506, 1993.

Nerem, R.S., B.D. Tapley, and C.K. Shum, Determination of the ocean circulation using Geosat altimetry, *J. Geophys. Res.*, *95*, 3163–3179, 1990.

Olbers, D., et al., *Hydrographic Atlas of the Southern Ocean*, 82 pp., Alfred Wegener Inst., Bremerhaven, Germany, 1992.

Olson, D.B., O.B. Brown, and S.R. Emmerson, Gulf Stream frontal statistics from Florida Straits to Cape Hatteras derived from satellite and historical data, *J. Geophys. Res.*, *88*, 4569–4577, 1983.

Olson, D.B., G. Podestá, R. Evans, and O. Brown, Temporal variations in the separation of Brazil and Malvinas Currents, *Deep Sea Res.*, *Part A*, *35*, 1971–1980, 1988.

Ou, H.W., and W.P.M. De Ruijter, Separation of an inertial boundary current from a curved coastline, *J. Phys. Oceanogr.*, *16*, 280–289, 1986.

Qiu, B., K.A. Kelly, and T.M. Joyce, Mean flow and variability in the Kuroshio Extension from Geosat altimetry data, *J. Geophys. Res.*, *96*, 18,491–18,507, 1991.

Schmitz, W.J., Jr., P.P. Niiler, and C.J. Koblinsky, Two year moored instument results along 152°E, *J. Geophys. Res.*, *92*, 10,826–10,834, 1987.

Shum, C.K., R.A. Werner, D.T. Sandwell, B.H. Zhang, R.S. Nerem, and B.D. Tapley, Variations of global mesoscale eddy energy observed from Geosat, *J. Geophys. Res.*, *95*, 17,865–17,876, 1990.

Tai, C.K., and W.B. White, Eddy variability in the Kuroshio Extension as revealed by Geosat altimetry, *J. Geophys. Res.*, *93*, 10,621–10,629, 1988.

Tai, C.K., and W.B. White, Eddy variability in the Kuroshio Extension as revealed by Geosat altimetry: Energy propagation away from the jet, Reynold stress, and seasonal cycle, *J. Phys. Oceanogr.*, *20*, 1761–1777, 1990.

Teague, W.J., M.J. Carron, and P.J. Hogan, A comparison between the Generalized Digital Environmental Model and Levitus climatologies, *J. Geophys. Res.*, *95*, 7167–7183, 1990.

Vazquez, J., V. Zlotnicki, and L-L. Fu, Sea level variabilities in the Gulf Stream between Cape Hatteras and 50° W: A Geosat study, *J. Geophys. Res.*, *95*, 17,957–17,964, 1990.

Visser, P.N.A.M., The use of satellites in gravity field determination and model adjustment, Ph. D. thesis, Delft Univ. of Technol., Delft, Netherlands, 1992.

Wakker, K.F., M.C. Naeije, R. Scharroo, and B.A.C. Ambrosius, Extraction of mesoscale ocean currents information from Geosat altimeter data, *Eur. Space Agency Spec. Pabl., ESA SP-312*, 221–226, 1990.

Watts, D.R., Gulf Stream variability, in *Eddies in Marine Science*, edited by A.R. Robinson, pp. 114–144, Springer-Verlag, New York, 1983.

Wesseling, P., *An introduction to Multigrid Methods*, 284 pp., John Wiley, New York, 1992.

Willebrand J., R.H. Käse, D. Stammer, H.-H. Hinrichsen, and W. Kraus, Verification of geosat sea surface topography in the Gulf Stream Extension with surface drifting buoys and hydrographic measurements. *J. Geophys. Res.*, *95*, 3007–3014, 1990.

Zlotnicki, V., Sea level differences across the Gulf Stream and Kuroshio Extension, *J. Phys. Oceanogr.*, *21*, 599–609, 1991.

R. C. V. Feron, Survey Department, Rijkswaterstaat, P.O. Box 5023, NL-2600 GA Delft, Netherlands. (e-mail: r.c.v.feron@mdi.rws.minvenw.nl)

W. P. M. De Ruijter and P. J. van Leeuwen, Institute for Marine and Atmospheric Research, Utrecht University, Princetonplein 5, NL-3584 CC Utrecht, Netherlands.

(Received February 13, 1995; revised August 12, 1996; accepted November 7, 1996.)